34th Annual International Conference of the IEEE EMBS
San Diego, California USA, 28 August - 1 September, 2012

Acquisition Information Spectrum for Evaluating Sonographic Quality

Nghia Q. Nguyen[1], Craig K. Abbey[2], and Michael F. Insana[3]

Abstract— **We are developing a first-principles task-based approach to the optimal design and evaluation of ultrasonic imaging systems. Examining five clinical features related to breast lesion diagnosis, we quantified information flow at several stages in the image formation process. We found that the diagnostic performance of a given system configuration will vary with the patient feature, sometimes significantly. Our analysis expresses diagnostic performance of an imaging system for a specific clinical task as a function of patient properties that are separable from instrument properties. Hence it is possible to show how image quality metrics, like spatial and contrast resolution, combine with patient features to determine feature discriminability. In this paper, we describe an information theoretic approach to diagnostic performance evaluation that has given us a new quantity, the *acquisition information spectrum (AIS)*. Like NEQ in radiography, AIS in sonography provides a foundation for medical ultrasonic imaging system design.**

I. INTRODUCTION

Assessments of image quality are most relevant when they predict the performance of instruments for accomplishing essential clinical tasks. Measurements of spatial and contrast resolution and noise properties are important but incomplete characterizations because they do not consider compromises among the metrics that are required to address various clinical task.

To develop a more comprehensive assessment, we model an ultrasonic imaging system as a device that transfers information from patients to medical decision makers (observers). Image quality, therefore, is based on the efficiency by which devices transfer specific task information. We focus on binary decisions made by observers between two classes of data that represent disease absence or disease presence. Observers can be expert humans or algorithms implementing decision theory. Of particular interest is the ideal observer, an algorithm that applies Bayes' Criterion (log-likelihood ratios) to generate scalar test statistics from image pairs that renders decisions guaranteed to meet the Neyman-Pearson minimum-error criterion of achieving the largest area under the ROC curve (AUC). In situations where the test statistic is normally distributed – the *normality condition* – it is now well known that the gold standard for system evaluation, AUC, can be related to the ideal observer signal-to-noise ratio (SNR_I) [1], and SNR_I^2 is a linear function of standard image quality metrics. Therefore the performance of a system at delivering clinical information can be predicted from properties of the clinical task and instrument properties.

The objective assessment of image quality was formalized for photon-based modalities during 1980s-1990s by Wagner, Barrett and others. Among the many prominent concepts to emerge is the SNR theory [1] that factorizes SNR_I^2 in the spatial frequency domain into patient features and instrument properties via the *noise-equivalent-quanta* (NEQ). NEQ is a product of three imaging system properties: large-area gray-scale transfer ($\tilde{H}$, contrast resolution), modulation transfer function (MTF, spatial resolution), and noise power spectrum (NPS). Through the normality condition, SNR analysis relates best-possible performance to instrument properties, which is the basis for modern radiographic and radionuclide imaging design and optimization [1], [2].

Unlike radiography, the formalisms underlying objective image assessment of sonography remain an open question. The biggest reasons are the post-beamforming nonlinear processing applied to sonographic images [3] and fundamental differences in object contrast: photon-based modalities encode contrast in the mean properties of tissues while sonography encodes contrast in the covariance matrix describing tissue properties. The ability of modern ultrasonic systems to allow access to beamformed RF echo data has enabled us to shift the analysis to the RF signal domain and avoid nonlinearities [4], [5]. Because contrast is found from the covariance matrix of stochastic tissue scatterers, the test statistic is a quadratic function of the RF data. This fact complicates the analysis by challenging the normality condition assumption. The effects are most pronounced for small-area diagnostic tasks, for example, those focused on lesion boundary discrimination.

To find solutions to these challenges, we adopted Kullback-Leibler entropy [7] in the definition of the diagnostic information contained within two classes of patient data. Information quantifies class separability in the form of the scalar divergence quantity, J. In this paper, we leverage the concept of NEQ from radiography to formulate an equivalent quantity for sonography based on J instead of SNR_I that loses meaning as normality is lost. We found a closed-form equation that shows how J can be used to link image quality metrics to task performance in sonography. AIS is a key component in describing the effectiveness of an ultrasonic system at transferring task information from the patient to RF data. Model observers and training human observers are used to reveal the efficiency of moving information from the RF signal into the image.

[1]N.Q. Nghia is with the Department of Electrical and Computer Engineering, University of Illinois at Urbana-Champaign, Urbana, IL 61801 USA nnguyen6 at illinois.edu

[2]C.K. Abbey is with the is with the Department of Psychology, University of California, Santa Barbara, CA 93106 USA abbey at psych.ucsb.edu

[2]M.F. Insana is with is with the Department of Bioengineering, University of Illinois at Urbana-Champaign, Urbana, IL 61801 USA mfi at illinois.edu

II. BACKGROUND

SIGNAL MODELING. We employ standard linear-system models of RF echo signal generation in sonography [4], [5]. RF echo vector $\mathbf{g}$ arises as a noisy discrete- space-to-discrete-time linear transformation from object/patient scattering vector $\mathbf{f}$ through matrix multiplication,

$$\mathbf{g} = \mathbf{H}\mathbf{f} + \mathbf{n} \; . \tag{1}$$

$\mathbf{H}$ is the system matrix and $\mathbf{n}$ is acquisition noise modeled by the zero-mean white Gaussian distribution, $\mathbf{n} \sim \mathcal{N}(0, \mathbf{\Sigma}_{\rm n})$, where noise covariance matrix $\mathbf{\Sigma}_{\rm n} = \sigma_{\rm n}^2\mathbf{I}$ and $\mathbf{I}$ is the identity matrix. $\mathbf{H}$ is constructed from a pulse-echo spatiotemporal impulse responses generated using the Field II program [8] with parameters selected to model a 1-D linear array from a Siemens Antares system. $\mathbf{f}$ is a vector assembled from a reformatted scattering object described as a zero-mean multivariate normal process, $\mathbf{f} \sim \mathrm{MVN}(\mathbf{0}, \mathbf{\Sigma}_{\rm obj})$. The nonstationary covariance matrix of the scattering object $\mathbf{\Sigma}_{\rm obj} = \sigma_{\rm obj}^2(\mathbf{I} + \mathbf{S}_i)$, where $\mathbf{S}_i$ encodes the lesion feature underlying data class i = 0, 1. $\mathbf{S}_0$ indicates a benign feature while $\mathbf{S}_1$ is a malignant feature. Task information is defined as $\Delta\mathbf{S} = \mathbf{S}_1 - \mathbf{S}_0$.

IDEAL OBSERVER. Because $\mathbf{f}$ is passed through a linear imaging system, $\mathbf{g}$ is also a zero-mean MVN process but with covariance matrix for the ith data class given by

$$\mathbf{\Sigma}_i = \sigma_{\rm obj}^2\mathbf{H}(\mathbf{I} + \mathbf{S}_i)\mathbf{H}^t + \sigma_{\rm n}^2\mathbf{I} \; . \tag{2}$$

Denoting $p_i(\mathbf{g})$ as the pdf for RF echo data from class i (the likelihood function), the ideal observer response to $\mathbf{g}$ is the logarithm of the likelihood ratio [2]

$$\lambda(\mathbf{g}) = \ln \frac{p_1(\mathbf{g})}{p_0(\mathbf{g})} \longrightarrow \frac{1}{2}\mathbf{g}^t(\mathbf{\Sigma}_0^{-1} - \mathbf{\Sigma}_1^{-1})\mathbf{g} \; . \tag{3}$$

The last form is obtained by removing terms unrelated to $\mathbf{g}$.

PERFORMANCE METRICS. The ideal observer compares its scalar test statistic λ to scalar threshold t when making decisions. From distributions $\lambda(\mathbf{g}|i)$, AUC is calculated and converted to detectability index d_A for comparing IO responses with other observers via

$$d_A = 2\mathrm{erf}^{-1}(2\mathrm{AUC} - 1) \; , \tag{4}$$

where erf$(\cdot)$ is the error function.

For normally distributed λ, $d_A = \mathrm{SNR}_I$, which is measured from the moments of λ [1], [2],

$$\mathrm{SNR}_I^2 = \frac{(E_1\{\lambda\} - E_0\{\lambda\})^2}{(\mathrm{var}_1\{\lambda\} + \mathrm{var}_0\{\lambda\})/2} \; . \tag{5}$$

where $E_i\{\lambda\}$ and $\mathrm{var}_i\{\lambda\}$ are means and variances of the test statistic for the ith class of data. Consequently, for normal λ, the three performance metrics are simply related by $\mathrm{SNR}_I = d_A = 2\mathrm{erf}^{-1}(2\mathrm{AUC} - 1)$.

III. ACQUISITION INFORMATION SPECTRUM

RADIOGRAPHY Wagner and Brown [1] derived an expression for SNR_I^2 in the 2-D spatial-frequency domain (u, v) of the image data. In radiography, where contrast is defined by variations in object mean, λ is a linear function of $\mathbf{g}$ and the normality of λ is reasonable to assume in all but extreme situations. They showed that ideal performance for photon-based imaging, SNR_I^2, is a linear function of the clinical task, $\Delta\tilde{S}(u,v)|^2$, and quality of the imaging instruments $\mathrm{NEQ}(u,v) = |\tilde{H}(0,0)|^2\,\mathrm{MTF}^2(u,v)/\mathrm{NPS}(u,v)$. That is,

$$\mathrm{SNR}_I^2 = \int_\infty du \int_\infty dv \; |\Delta\tilde{S}(u,v)|^2 \,\mathrm{NEQ}(u,v) \; . \tag{6}$$

The derivation assumes a linear shift-invariant (LSI) system, stationary noise, and the task of discriminating low-contrast circular lesions from a constant-mean background. NEQ combines instrument properties into one quantity that characterizes the ability of the instrument to transfer object contrast into recorded data at each frequency channel. Combining (5) and (6), we see how performance obtained from observer measurements are related to predictions based on instrument properties.

SONOGRAPHY Eq (3) shows that λ is a quadratic function of $\mathbf{g}$. For MVN echo data, λ is thus described by a χ^2 distribution [6]. When observers view image data where the task extends spatially over an area large compared with the correlation length of the image data, the Central Limit Theorem allows us the assume normal λ. For lesion boundary discrimination, where the task is distributed over a small area in the image data, the CLT does not ensure normality. Hence SNR_I^2 loses relevance since its relationship with d_A and AUC is unknown.

In sonography, detectability is better described by the Kullback-Leibler divergence J. To derive an expression analogous to (8) for sonography, we write J in terms of class covariances and then image quality parameters. For two class distributions of RF echo data with zero mean and covariance matrices $\mathbf{\Sigma}_i$ [9],

$$J = \frac{1}{2}\mathrm{Tr}\left[\left(\mathbf{\Sigma}_0^{-1} - \mathbf{\Sigma}_1^{-1}\right)\left(\mathbf{\Sigma}_1 - \mathbf{\Sigma}_0\right)\right] \; . \tag{7}$$

Inverting large matrices is achieved by a power series expansion [4]. Limiting our study to low-contrast feature detection we can truncate the series expansion after the first term to approximate (7) in closed form as

$$J \approx \frac{1}{2}\mathrm{Tr}\left[\mathbf{\Sigma}_s^{-1}\left(\Delta\mathbf{\Sigma}_1 - \Delta\mathbf{\Sigma}_0\right)\mathbf{\Sigma}_s^{-1}\left(\mathbf{\Sigma}_1 - \mathbf{\Sigma}_0\right)\right] \; , \tag{8}$$

where

$$\begin{aligned} \mathbf{\Sigma}_s &= \sigma_{\rm obj}^2\mathbf{H}\mathbf{H}^t + \sigma_n^2\mathbf{I} \; , \\ \Delta\mathbf{\Sigma}_i &= \sigma_{\rm obj}^2\mathbf{H}\mathbf{S}_i\mathbf{H}^t \; . \end{aligned} \tag{9}$$

Since we will use J in place of d_A^2, we obtain from (8),

$$d_A^2 \approx \frac{1}{2}\mathrm{Tr}\left[\mathbf{K}_s\Delta\mathbf{S}\mathbf{K}_s\Delta\mathbf{S}\right] \; , \tag{10}$$

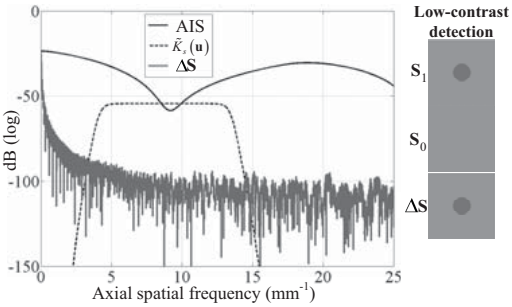

Fig. 1. One-dimensional AIS(u) and $\widetilde{K}_s(u)$ curves are plotted versus spatial frequency along the beam axis for the task of lesion detection.

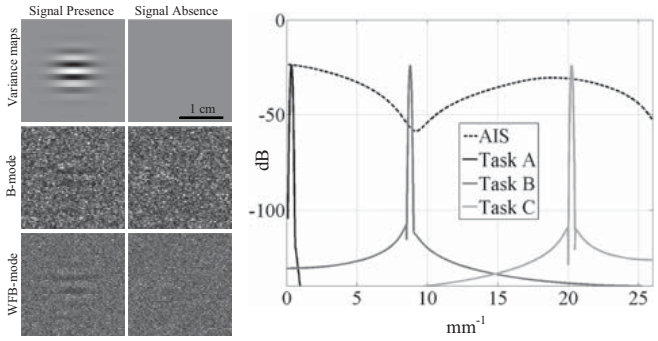

Fig. 2. (Left) Variance masks of the sine-wave detection task (Top), and examples of B-mode (middle) and WFB-mode (bottom) images. (Right) The AIS with task information over the axial spatial frequency. Task A is at 0.35 (mm^{-1}) corresponding to the map variance in the left, Task B is at 8.77 (mm^{-1}) and Task C is at 20.24 (mm^{-1}).

where $\mathbf{K}_s \triangleq \mathbf{H}^t\mathbf{\Sigma}_s^{-1}\mathbf{H}$ and now $\Delta\mathbf{S} = \sigma^2_{\text{obj}}(\mathbf{S}_1 - \mathbf{S}_0)$ defines task information.

Under the LSI/stationary assumptions, $\mathbf{K}_s$ can be diagonalized using Fourier techniques as $\mathbf{K}_s = \mathbf{F}^{-1}\widetilde{\mathbf{K}}_s\mathbf{F}$, where $\mathbf{F}$ is the forward DFT matrix [2]. Since $\widetilde{\mathbf{K}}_s$ is diagonal, its elements can be represented by a single index, $\widetilde{\mathbf{K}}_s(k,k) = \widetilde{\mathbf{K}}_s(k)$. Similarly, $\Delta\mathbf{S} = \mathbf{F}^{-1}\Delta\widetilde{\mathbf{S}}\mathbf{F}$, and therefore (10) is expressable as a double sum over frequency indices

$$\begin{aligned} d_A^2 &\simeq \frac{1}{2}\text{Tr}\left[\widetilde{\mathbf{K}}_s\Delta\widetilde{\mathbf{S}}\widetilde{\mathbf{K}}_s\Delta\widetilde{\mathbf{S}}\right] \\ &= \frac{1}{2}\sum_k\sum_l \widetilde{K}_s(k)\Delta\widetilde{S}(k,l)\Delta\widetilde{S}(l,k)\widetilde{K}_s(l). \quad (11) \end{aligned}$$

Since $\Delta\mathbf{S}$ is diagonal, $\Delta\widetilde{\mathbf{S}}$ is Hermitian and stationary, i.e. $\Delta\widetilde{S}(l,k) = \Delta\widetilde{S}^*(k,l) = \Delta\widetilde{S}(l-k)$, in which $\Delta\widetilde{S}(k)$ is the Fourier transform of $\Delta\mathbf{S}$ but re-arranged into a column vector before taking the transform.

Expressing (11) as a continuous function of 2-D spatial frequency variable, $\mathbf{u} = (u,v)$, we have

$$\begin{aligned} d_A^2 &\simeq \frac{1}{2}\int_\infty d\mathbf{u}\int_\infty d\mathbf{u}'\ \widetilde{K}_s(\mathbf{u}')\left|\Delta\widetilde{S}(\mathbf{u}-\mathbf{u}')\right|^2\widetilde{K}_s(\mathbf{u}) \\ &= \int_\infty d\mathbf{u}\left|\Delta\widetilde{S}(\mathbf{u})\right|^2\left\{\frac{1}{2}\widetilde{K}_s(\mathbf{u}')*\widetilde{K}_s(-\mathbf{u}')\right\}(\mathbf{u}) \\ &= \int_\infty d\mathbf{u}\left|\Delta\widetilde{S}(\mathbf{u})\right|^2\text{AIS}(\mathbf{u}) \triangleq d^2_{Ks}\,. \quad (12) \end{aligned}$$

where $\widetilde{K}_s$ is given by

$$\widetilde{K}_s(u,v) = \frac{\left|\widetilde{H}(u,v)\right|^2}{\left|\widetilde{H}(u,v)\right|^2\sigma^2_{\text{obj}} + \sigma^2_{\text{n}}}\,. \quad (13)$$

Comparing (12) to (6), we find performance in both cases depends on task contrast $|\Delta\widetilde{S}|^2$. However the autocorrelation function of $\widetilde{K}_s$, we call is the acquisition information spectrum or AIS$(\mathbf{u})$, serves the role in sonography that NEQ$(\mathbf{u})$ does in radiography. It provides an avenue for relating image quality metrics to task information.

AIS$(\mathbf{u})$ provides a rigorous connection between task information and image quality parameters. It may be interpreted as the number of independent samples of task information being offered to the observer at spatial frequency $\mathbf{u}$. $\widetilde{K}_s(\mathbf{u})$ in Eq. (13) resembles a generalized NEQ quantity [2] for photon imaging in a variable background. Here acoustic speckle in the RF signal is considered to be a random background. $\widetilde{K}_s(\mathbf{u})$ is analogous to GNEQ [2] but there are important differences. First, the background randomness described in (13) is always present in sonography because it is due to coherent speckle present in the RF echo signal. Second, since AIS $= \frac{1}{2}\text{ACF}(\widetilde{K}_s)$ and not $\widetilde{K}_s$, there is a broader system responsiveness to object contrast than one expects from MTF$(\mathbf{u}) = |H(\mathbf{u})|/|H(\mathbf{0})|$ alone. Also the bandpass nature of the RF echoes means that AIS always has three lobes centered at zero frequency (see Fig. 1).

IV. INFORMATION LOSS OVER THE SPATIAL FREQUENCY SPECTRUM

In radiography, NEQ is proportional to the MTF^2. It is maximum at the origin and generally decreases at higher spatial frequencies, reflecting the degradation of image quality as the demand for spatial resolution increases. In sonography, AIS is maximum at zero frequency but its curve has three lobes formed from the bandpass nature of RF echo signals (see Fig. 1). The central main lob has amplitude information and the sidelobes contain phase information present in RF signals but not in sonograms. In this section, we are interested in (a) validating the curve for the AIS of RF data and (b) learning how information is lost during echo demodulation.

To validate the AIS prediction, we applied the ideal (IO) and Smith-Wagner (SW) computational observers to data simulations to study the relative loss of information caused by echo demodulation. SW is the ideal observer for low-contrast sonographic lesion detection [3], and is sub-optimal and human-like for other tasks [4]. Both observers were tasked with detecting sinusoidal modulations in object scattering variance using a narrow-band task [10]. These tasks were Gabor pulses that became the variance masks as shown in Fig. 2 (left, top). The amplitude of the Gabor pulse is set at -25 dB of the background to guarantee a low-contrast task. Setting the carrier frequency of the Gabor pulse to low frequency, we plot the resulting task function $|\Delta\widetilde{S}(\mathbf{u})|^2$ in the

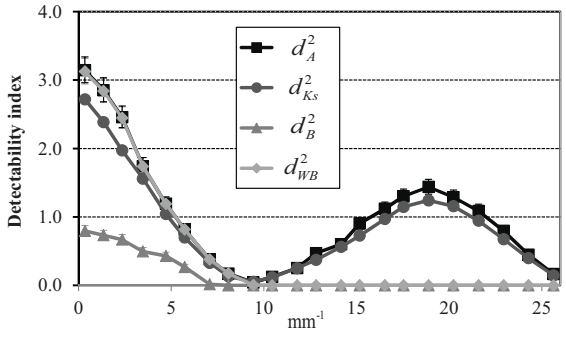

Fig. 3. Comparisons among the detectability indices d_A^2 converted from area under ROC of the ideal observer, d_{Ks}^2 calculated from Eq. (12), and d_B^2 and d_{WB}^2 calculated from the performance of the Smith-Wagner observer.

Fourier domain on the right labeled Task A. By increasing the carrier frequency, we were able to sweep the task over a broad range of spatial frequencies. At each frequency u_0, index d_{Ks}^2 is calculated through Eq. (12) for $|\Delta\widetilde{S}(\mathbf{u})|^2 \simeq A^2\delta(u-u_0,0)$. The narrow-band response meant the Gabor pulse approximates a Dirac delta for sampling value of the AIS curve. When frequency sampling is dense enough, the AIS curve can be mapped discretely in terms of d_{Ks}^2, and measured and predicted values for AIS can be compared as in Fig. 3.

For each value of u_0, 2000 pairs of RF signals are generated for observers to view when calculating detectability indices. IO performance is converted to d_A^2 using RF echo data and compared with d_{Ks}^2. SW observers viewing the B-mode images generated from the same echo data gave responses that we represent by the detectability index d_B^2. We also Wiener filtered the RF echo data before computing B-mode images and used SW observer to estimate performance denoted by d_{WB}^2. An example of B-mode and WFB-mode images for the variance maps are shown in Fig. 2(left, middle and bottom). The indices are also plotted in Fig 3.

V. DISCUSSION

Larger values of detectability indices reported in Fig. 3 represent superior task performance. Measured ideal performance d_A^2 is very similar to that predicted by d_{Ks}^2, which suggests the shape of AIS plotted in Fig. 1 is what can be expected experimentally. Both curves have peaks at origin and at 18.89 mm^{-1}, and both have a minimum at 9.44 mm^{-1}. The location of maxima and minima depend on the bandwidth and center frequency of the ultrasound pulse. Predicted performance values, d_{Ks}^2, are 7-9% lower than measurements via d_A^2 and yet the corresponding AUC values agree within 2%. Thus AIS is a realistic representation of instrument properties, as distinct from patient features, and these two quantities can be combined in the frequency domain to predict task-dependent system performance.

Note that d_B^2 is reduced to about 25% of d_A^2, suggesting that 75% of task information is lost through demodulation. The shape of d_B^2 monotonically decreases as we see with NEQ in photon imaging because sonography uses base-band data that discards high frequency sensitivity. d_B^2 is reduced to zero at 7-9 mm^{-1} with the loss of phase information because of spatial resolution limitations. Image speckle blocks the object details at frequencies higher than 9 mm^{-1}. Wiener filtering the echo signal before modulation recovers most of the information in the first lobe of the AIS curve ($d_{WB}^2 \simeq d_A^2$), but the system cannot respond to high frequencies because of demodulation. Recovering patient information lost to demodulation is a subject of future investigation.

In this paper, we propose AIS as a fundamental quantity for relating instrument properties to task performance. The nature of sound tissue interactions changes the source of object contrast in sonography, which means that AIS has a more complicated frequency structure than NEQ in radiography. The information theoretic approach described here is intended to provide a rigorous foundation for evaluating and optimizing sonographic systems used for medical diagnosis. Although this treatment is focused on the acquisition stage of image formation, the display stage must also be addressed to predict overall clinical performance. The ideal-observer analysis can help designers adjust acquisition parameter to maximize RF data information, but human observer studies are needed to ensure accessibility of the information to human observers.

ACKNOWLEDGMENT

This work is supported by NIH under award No. CA118294.

REFERENCES

[1] R.F. Wagner and D.G. Brown, "Unified SNR analysis of medical imaging systems," *Phys Med Biol*, vol 30, pp.489-518, 1985.
[2] H.H. Barrett and K.J. Myers, *Foundations of Image Science*. Hoboken, NJ: John Wiley & Sons, 2004.
[3] S.W. Smith, R.F. Wagner, J.M. Sandrik, and H. Lopez, "Low contrast detectability and contrast/detail analysis in medical ultrasound," *IEEE Trans Son Ultrason*, vol. 30, no. 3, pp. 164-173, May 1983.
[4] C.K. Abbey, R.J. Zemp, J. Liu, K.K Lindfors, M.F. Insana, "Observer efficiency in discrimination tasks simulating malignant and benign breast lesions with ultrasound," *IEEE Trans Med Imag*, vol. 25, no. 2, pp. 198-209, Feb. 2006.
[5] N.Q. Nguyen, C.K. Abbey, M.F. Insana, "An adaptive filter to approximate the Bayesian strategy for sonographic beamforming," *IEEE Trans Med Imag*, vol. 30, no. 1, pp. 28-37, Jan. 2011.
[6] N.Q. Nguyen, C.K. Abbey, M.F. Insana, "Detectability index describes the information conveyed by sonographic images," *in Proceedings of IEEE Ultrasonics Symposium*, Orlanda, October, 2011 (in press).
[7] S. Kullback, R.A. Leibler, "On information and sufficiency," *Annals of Math Stat*, vol. 22 no. 1, pp. 7986, 1951.
[8] J.A. Jensen and N.B. Svendsen, "Calculation of pressure fields from arbitrarily shaped, apodized, and excited ultrasound transducers," *IEEE Trans Ultrason Ferroelec Freq Control*, vol. 39, no. 2, pp. 262-267, 1992.
[9] K. Fukunaga, *Introduction to Statistical Pattern Recognition, 2/e*. New York, NY: Academic Press, 1990.
[10] A. Burgess and H. Ghandeharian, "Visual signal detection. I. Ability to use phase information," *J Opt Soc Am A*, vol. 1, no. 8, pp. 900-905, 1984.